scientific reports

Check for updates

OPEN

A new in vitro pre-clinical method for testing SARS-CoV-2 nasopharyngeal swabs

Ian Camilo Orjuela-Garzón[1]✉, Inés María Fernández-Calderón[1], María de los Ángeles Ayala[1], María Alejandra Rodríguez Soto[1], Camilo Eduardo Pérez-Cualtán[1,2], Camila Irene Castro-Paez[1,2], Juan C. Cruz[1], Carolina Muñoz-Camargo[1], Javier Navarro[2,3], Rodrigo Cabrera[4,5] & Juan C. Briceño[1,2,6]

The SARS-CoV-2 pandemic underscored the critical role of nasopharyngeal swabbing in virus detection and containment. The urgency for mass production of swabs highlighted the necessity to evaluate their efficiency against the global shortage of medical supplies. Traditional pre-clinical swab testing methods often overlook the complexities of the nasopharyngeal anatomy and mucus properties. This study introduces an innovative in vitro pre-clinical model using a 3D-printed nasopharyngeal cavity lined with a mucus-mimicking SISMA hydrogel, to generate a novel assessment protocol for nasopharyngeal swab efficiency. Reconstructing nasopharyngeal anatomy from CT images, the model used flexible and rigid resins to simulate soft tissue and bone properties. Our evaluation compared the sample collection and release performance of experimental Heicon-type injection-molded swabs and conventional nylon flocked swabs. The Heicon swabs exhibited superior SISMA release efficiency, compared to the standard tubular model. Both swab types demonstrated lower cycle threshold (Ct) values in the tubular model, indicative of higher viral load retrievals. RT-qPCR results confirmed these differences and validated the hydrogel's suitability as a mucosa equivalent. The findings support using our nasopharyngeal model, which better simulates clinical conditions, potentially improving swab design and the reliability of viral detection assays.

Keywords Pre-clinical model, Nasopharyngeal swabs, *In vitro* testing, SARS-CoV-2, yellow fever

Amid the SARS-CoV-2 pandemic, the global healthcare system faced a myriad of challenges, not least among them was a critical shortage of supplies, including nasopharyngeal swabs for collection of mucosal samples essential for viral detection[1]. This scarcity impeded containment strategies and highlighted the development of alternative swab designs and manufacturing methods, including injection molding and stereolithography[2]. Yet, these innovative biomedical devices demand rigorous validation, particularly in terms of their efficacy for adequate sample collection and release, in comparison to established commercial products.

Common pre-clinical testing for nasopharyngeal swabs involves immersing the swab in saline solutions or employing volunteers for cheek swabbing[1]. These methods, while straightforward, fail to account for the complex anatomy of the nasopharyngeal cavity, the unique properties of mucus, and the specific technique required for nasopharyngeal sample collection. A more sophisticated pre-clinical testing should not only evaluate the swab's ability to absorb and release samples but also replicate the anatomical and rheological difficulties inherent in the swabbing process[1,2].

Additionally, accurate and consistent sample collection is a keystone of effective swabbing, since it could result in false-negatives which compromise sensitivity and reliability of the test[1,2]. These diagnostic failures may lead to missed or delayed diagnoses, which creates an impairing of the treatment, isolation, and ultimately affects the patient's outcomes and public health system. In the context of pandemics and epidemics of respiratory viruses,

[1]Department of Biomedical Engineering, Universidad de los Andes, Cra. 1 Este N° 19A 40, Bogotá 1117111, DC, Colombia. [2]Center for Modeling and 3D Printing, Fundación Cardioinfantil-Instituto de Cardiología, Bogotá, Colombia. [3]Department of Surgery, Medical School, Visible Heart Labs, University of Minnesota, Minneapolis, United States. [4]Center for Research in Genetics and Genomics (CIGGUR), GENIUROS Research Group, School of Medicine and Health Sciences, Universidad del Rosario, Bogotá, Colombia. [5]Molecular Biology and High Complexity Diagnosing Testing Laboratory, Fundación Cardioinfantil-Instituto de Cardiología, Bogotá, Colombia. [6]Department of Research, Fundación Cardioinfantil-Instituto de Cardiología, Bogotá, Colombia. ✉email: ic.orjuela@uniandes.edu.co

it hinders epidemiological surveillance to have an efficient response to the emergency[1]. Suboptimal swabbing can arise from different factors such as complex nasopharyngeal anatomy, variability in operator technique, swab design, and mucus characteristics such as viscoelasticity and shear-thinning properties[1–4]. These variables highlight the need for realistic and standardized pre-clinical models to evaluate swab performance under controlled yet physiologically relevant conditions.

Added to the shortage of swabs supplies, low- and middle-income countries concurrently struggled with constraints in characterizing, evaluating, validating, and regulating new medical products[5]. In Colombia, for instance, numerous companies began to develop and manufacture nasopharyngeal swabs such as 3D Solutions[6]. However, because of such limitations, the translation of these products into clinical use has been stymied[7]. In response to these critical issues, the aim of this study was to design and manufacture a novel in vitro pre-clinical test bench nasal cavity that emulates the human nasal cavity, thereby facilitating a more authentic evaluation of nasopharyngeal swab performance for sample collection and viral detection by reverse transcription-quantitative polymerase chain reaction (RT-qPCR). Our model, which closely mimics the anatomical features and mucus consistency of the nasopharyngeal cavity, was used to compare the performance of experimental nasopharyngeal swabs manufactured by Plastinovo S.A.S. (La Estrella, Colombia) via one-step injection-molding technique, against commercially available swabs with identical dimensional specifications from HanChang Medic Co. Ltd (Seoul, Korea) and Changzhou Munk Foam Technology Co. Ltd (Jiangsu, China). The aim was not only to assess efficacy in sample collection but also to ensure a realistic representation of the swabbing process, thereby providing a more accurate pre-clinical validation of these essential biomedical devices. Underlying this effort is the hypothesis that a physiologically relevant in vitro platform can better differentiate swab performance and thus serve as a more reliable tool to guide both swab design improvements and preclinical testing.

Results

3D printed nasopharyngeal cavity model

Head CT scans of patients allowed the anatomically accurate reconstruction of hard and soft tissues of the nasopharyngeal region (Fig. 1a). This model was crafted using dual-material 3D printing techniques, using hard VeroBlue™ for bone-mimicking rigidity and Agilus30™ for soft tissue flexibility (Fig. 1b). The blue rigid VeroBlue with a modulus of elasticity between 2.2 and 3.0 GPa[8] is close to the values found for the bones of the human orbital wall (2.14–2.36 GPa)[9]. On the other hand, the translucent flexible Agilus30 with Shore hardness values close to 40 on the A scale[10] mirrors those of hyaline cartilage (50–60 on the A scale)[11]. The combination of these two materials confers a high degree of structural fidelity to the model. The realistic deformation response to swab insertion, restrained by the model's bony framework (Fig. 1c), underscores the model's physiological relevance. Additionally, the chosen SISMA hydrogel simulates nasopharyngeal mucus with remarkable precision, showcasing shear-thinning behavior and viscosity parameters nearly identical to actual mucosa i.e[12]. , close to 10 Pa·s at low shear rates[3]. Figure 2 shows the rheological comparison between the SISMA hydrogel and sinus nasal mucus[4], indicating a similar viscosity behavior with changes on shear rate and similar values of n (0.234 for SISMA and 0.187 for mucus).

Validation of collection-release capacities of the swabs

The swab comparison involved commercial (nylon flocked) and novel Heicon (injection-molded) variants (Fig. 3a). The commercial swab collected 1.8 and 3.2 times more SISMA than the Heicon swab in the nasopharyngeal cavity model and tube standard, respectively. It was also found that the Heicon and commercial swabs collected 4.8 and 8.4 times more SISMA in the tube model than in the cavity. This disparity aligns with existing literature, where flocked swabs outperform injection-molded swabs in similar tests, likely due to the hydrophobic characteristics of the latter, which impede material absorption[13].

When comparing the amount of SISMA released between models, both swab types exhibited significantly greater release in the tube standard than in the nasopharyngeal cavity model. Specifically, the commercial swab released approximately 3.2 times more hydrogel in the tube than in the cavity (49.99 ± 13.89 µL vs. 15.81 ± 4.21 µL), while the Heicon swab released approximately 4.0 times more (40.94 ± 5.13 µL vs. 10.31 ± 3.70 µL). These differences underscore the increased challenge posed by the anatomical and physiological barriers of the cavity model, which reduce swab performance despite using the same sampling protocol. It is important to highlight that there is a statistically significant difference between the two models for both swabs (commercial and Heicon in cavity v. in tube, $p < 0.0001$).

The use of the nasopharyngeal cavity model led to a considerable improvement in sample release efficiency compared to the standard tube model. For the Heicon swabs, the cavity model allowed a 1.2-fold increase in release percentage ($82.48 \pm 12.70\%$ vs. $68.77 \pm 8.49\%$), while for the commercial swabs, the improvement was even more pronounced, with the cavity model yielding a 2.7-fold increase ($69.44 \pm 12.68\%$ vs. $25.89 \pm 6.76\%$). There is a statistically significant difference between the two swab models for both protocols ($p < 0.0001$ using tube; $p = 0.0470$ using cavity) as well as between the results obtained in tube and cavity for both swabs ($p = 0.0281$ for Heicon; $p < 0.0001$ for commercial). These results confirm that the anatomical complexity of the cavity model facilitates more effective interaction and release dynamics than the simplified tube setup. These findings are summarized in Table 1, which compares collected and released sample volumes, and release percentages for both swabs across both models.

In comparison to reported data, effective release percentages were 24% for a flocked swab and 60% for a swab developed by additive printing, which closely resembles the trends observed here[14]. Nevertheless, that data was collected using a simplified tube model, without recapitulating the complexity of the clinical nasopharyngeal sampling protocol. Overall, the data collected evidenced that the Heicon swab is an alternative that provides better release percentages compared to the commercially available swabs.

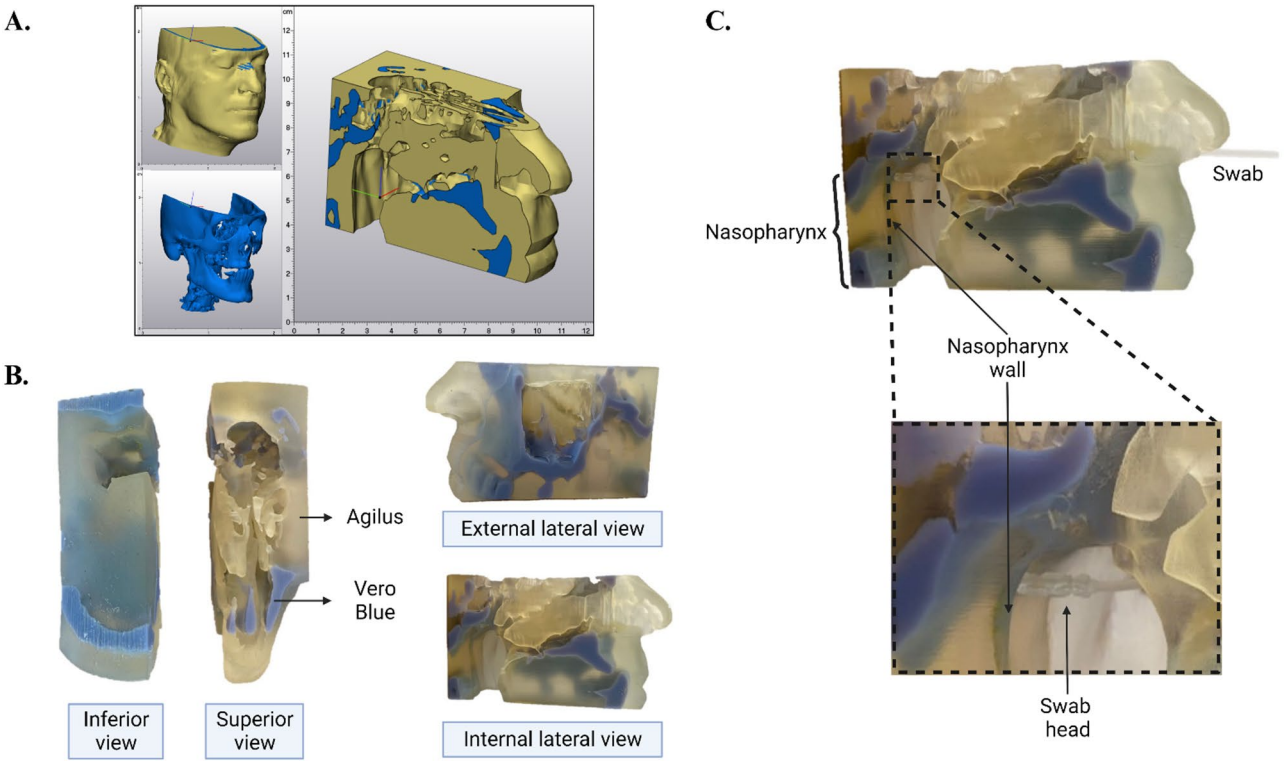

Fig. 1. 3D printed nasopharyngeal cavity model. (**a**) The computational segmentation of CT images allowed the reconstruction of the bone and soft tissues of the head. Blue indicates bony structures, and gold represents soft tissue regions such as mucosa and nasal septum. (**b**) Nasopharyngeal segment 3D printed using two different materials (VeroBlue™ and Agilus30™) to account for the difference between the elastic properties of bone and soft tissues. The materials were selected to mimic the mechanical behavior of each tissue type, with VeroBlue™ mimicking bone and Agilus30™ mimicking cartilage and mucosa. The inferior, superior, internal and external view of the cavity views of the 3D printed nasopharyngeal cavity model. (**c**) The swab (Heicon swab shown in the images) is introduced into the nostril and pushed all the way back until it touches the wall of the nasopharynx. The 3D renderings in panel (**a**) were created by the authors using Mimics® (version 24.0, Materialise NV, Leuven, Belgium, https://www.materialise.com/en/healthcare/mimics) and 3-Matic® (version 16.0, Materialise NV, Leuven, Belgium, https://www.materialise.com/en/industrial/software/3-matic).

Viability of the swabs for adequate virus-loaded sample collection

In YFV-loaded SISMA assays, the Heicon swab showed a Ct of 30.08 in the cavity and 25.91 in the tube, corresponding to a difference of 4.17 cycles, or roughly a 20-fold decrease in detected RNA due to the anatomical complexity. The commercial swab showed a Ct of 31.48 in the cavity and 26.69 in the tube, a difference of 4.79 cycles, which corresponds to more than a 25-fold decrease. These statistically significant differences quantitatively demonstrate the challenge of sample retrieval in anatomically accurate conditions ($p < 0.0001$ for Heicon and commercial). The Ct values indicated comparable viral material detection between swab types, irrespective of the model used ($p = 0.1734$). This equivalence suggests that Heicon nasopharyngeal swabs have a comparable performance to commercial swabs in terms of quantifiable viral sample retrieval (Fig. 4a).

The PCR results for the YFV-loaded SISMA validated that the mucosal model chosen is compatible with single-stranded viral material embedded in a capsid at a specific concentration of 5000 copies/mL and that the presence of a capsid does not prevent adequate RNA extraction. The Ct values obtained were consistently below the clinical detection threshold of 40 and demonstrated statistically significant differences between cavity and tube models ($p < 0.0001$), confirming the ability of the hydrogel to mimic mucosal retention and release properties. In relation to nasopharyngeal swabs, it is evident that both types obtain comparable amounts of quantifiable viral material. However, the standard model showed a significantly lower genetic material recovery compared to the nasopharyngeal cavity model, which could indicate significant discrepancies with respect to the actual nasopharyngeal test. Thus, this may impact the reliability of swab approvals for clinical use, as the anatomical model offers a more accurate representation of in vivo conditions.

Final validation of the test bench for nasopharyngeal swab evaluation was established by depositing SARS-CoV-2-loaded SISMA on the nasopharyngeal cavity, followed by the swabbing test. As shown in Fig. 4B, in the cavity model, Heicon swabs yielded Ct values of 27.68 ± 1.16 (FAM) and 27.00 ± 2.86 (HEX), whereas commercial swabs showed 28.41 ± 0.93 (FAM) and 28.64 ± 1.41 (HEX). In the tube model, Ct values decreased for both swabs, with Heicon registering 22.89 ± 2.20 (FAM) and 23.59 ± 2.99 (HEX), and commercial swabs 24.82 ± 0.93 (FAM) and 24.52 ± 0.97 (HEX). These differences translate to approximately 28.0-fold and 12.0-fold increases

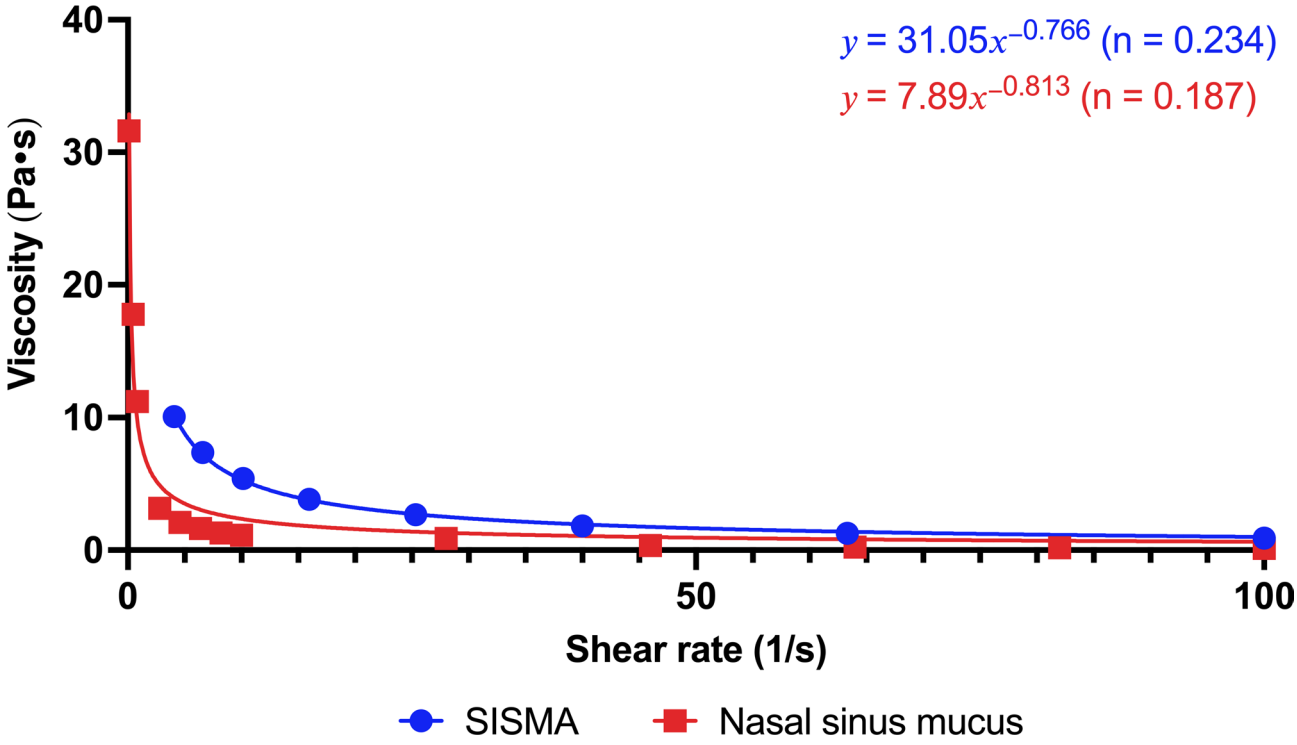

Fig. 2. Flow sweep power-law model fitting of SISMA and nasal sinus mucus data with its associated n coefficient.

in detectable nucleic acid (for Heicon and commercial swabs respectively in FAM), and 10.6-fold and 17.3-fold increases (in HEX), when moving from the cavity model to the tube model. These low statistical differences (FAM and HEX channels in cavity v. in tube, $p = 0.0048$ for Heicon and $p = 0.0295$ for commercial) indicate that the sampling environment affects nucleic acid recovery, with tube models overestimating performance. Likewise, there is no statistically significant differences between the FAM and HEX channels of both swabs for the tube and cavity models (Heicon v. commercial in cavity and tube, $p > 0.1523$). Nevertheless, the Ct values for both swabs in the tube and cavity models do not exceed the acceptance limit of 40, so it can be stated that the results found have adequate clinical relevance. A study developed in a model tube with PBS loaded with SARS-CoV-2 at a concentration of 10^3 copies/mL found that Ct values are between 35 and 40 for swabs[15], which could be related to the low viscosity of the solution used therein. The complete quantitative summary is presented in Table 2.

Discussion

This study has successfully established a digitally reconstructed nasopharyngeal cavity model utilizing VeroBlue™ and Agilus30™ to accurately replicate the rigidity and flexibility of the cavity's soft and hard tissues. Incorporated within this model, SISMA hydrogel was meticulously selected to emulate the elastic modulus of biological tissues and the viscosity essential for mucociliary transport, thereby authentically simulating the anatomical intricacies of the nasopharyngeal environment. The investigation revealed significant disparities in the sample collection and release performances between commercial flocked and injection-molded swabs, as evidenced by RT-qPCR data. The mechanical properties of each material allow the model to present a higher degree of anatomical and physiological accuracy, as the nasal cavity maintains its structure thanks to the bony and cartilaginous framework[16].

Most nasopharyngeal swab tests consist of tubes with high viscosity liquid solutions that attempt to recreate the human mucosal properties but lose the anatomical details[17,18]. Other studies reported the use of rigid and/or flexible reconstructions of the nasopharyngeal cavities without a solution to replicate the internal lining of the nasal tract[19,20]. A model that involves most of these parameters is a 3D printed cavity in rigid ABS material with an internal sponge that simulates mucus in the nasopharyngeal area[1]. However, the fact that the entire nasal passage is made of a rigid material means that the heterogeneous anatomical properties physiologically observed are lost and can lead to significant changes in the sample collection results of the nasopharyngeal swabbing procedure. Overall, this nuanced reproduction of the nasal passages' anatomy and rheology represents a significant enhancement over existing models, which lack either anatomical detail or appropriate mucosal mimicry. Our 3D nasopharyngeal model combines anatomical realism (derived from CT imaging of the upper airway) with functional features such as soft-tissue-mimicking materials and a hydrogel-coated epithelial surface to simulate mucus. This setup enables repeatable evaluation of both swab collection and release under physiologically relevant conditions. Compared to flat or tubular models, it provides a more stringent and

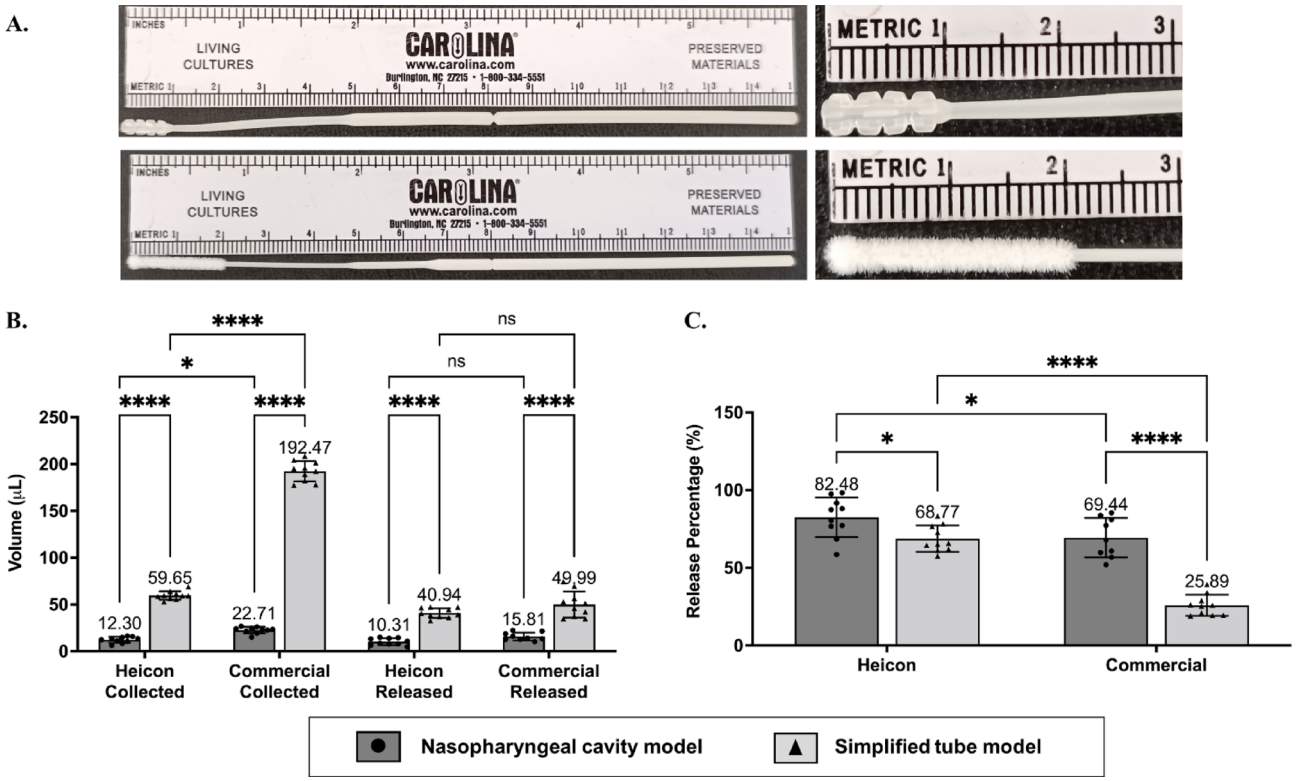

Fig. 3. (**a**) Novel Heicon-type swabs (top) manufactured via one-step injection assessed using the protocol proposed; the head has 11 mm length and 2.2 mm diameter. In comparison, commercial nylon flocked swabs (bottom, Changzhou Munk Foam) have a head of 20 mm length and 2 mm diameter. (**b**) Collected and released sample volumes for the Heicon and Commercial swabs using the nasopharyngeal cavity (dark grey columns) or the simplified tube (light grey columns) models. (**c**) The release percentage, the relative amount of sample released from the collected volume for Heicon and commercial swabs in the nasopharyngeal cavity and tube models. Experiments were performed ten times (ns is $p > 0.1234$, * is $p \leq 0.1234$, ** is $p \leq 0.0332$, *** is $p \leq 0.0021$, **** is $p < 0.0001$).

Model	Swab type	Collected volume (µL ± SD)	Release volume (µL ± SD)	Release percentage (% ± SD)
Cavity	Heicon	12.30 ± 3.24	10.31 ± 3.70	82.48 ± 12.70
	Commercial	22.71 ± 3.40	15.81 ± 4.21	69.44 ± 12.68
Tube	Heicon	59.65 ± 4.49	40.94 ± 5.13	68.77 ± 8.49
	Commercial	192.47 ± 10.82	49.99 ± 13.89	25.89 ± 6.76

Table 1. Collected and released sample volumes, and release percentages for Heicon and commercial swabs in the nasopharyngeal cavity and tube models.

realistic test environment for swab tip interaction, trajectory control, and target site access. However, limitations remain, including the absence of mucociliary dynamics and the time-dependent behavior of hydrogels, which may require replenishment or rehydration across multiple test cycles.

In terms of the collection-release capacities, the commercial swab demonstrated superior collection capacity over the Heicon swab, with notable discrepancies observed between the tube standard and the nasopharyngeal cavity model (Fig. 3b). In relation to the use of a standard tube model, the literature shows an increase in the volume of sample collected compared to simple anatomical models, but the standard model protocol usually demands larger volumes of fluid compared to anatomical models[1]. The discrepancy in sample collection between standard and anatomical models confirms the importance of using a validation methodology for nasopharyngeal swab collection processes that better recreates the anatomy in which the procedure is performed for the intended use. Unlike the methodology adopted in this study, others have reported the use of fluorescent-labeled particles to mimic the cellular material that is released into the transport medium[1,13]. However, in a study conducted by Tay and collaborators[14], where the performance of flocked and 3D printed, swabs were compared using a tube model, it was established that both swabs released a similar volume of a mucus analogue that was based on an aqueous solution of Pluronic F127 25% (w/v). Considering its function, it is important that a nasopharyngeal

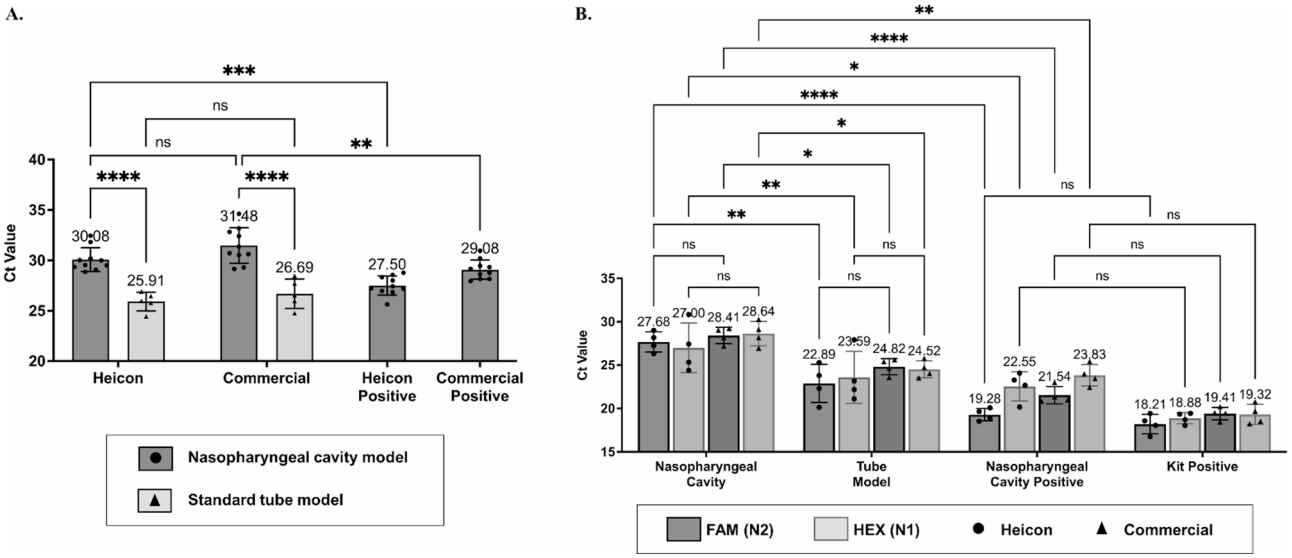

Fig. 4. RT-qPCR Ct values for RNA from (**a**) YFV taken with Heicon and Commercial nasopharyngeal swabs from both tube and cavity models; and (**b**) SARS-CoV-2 taken with Heicon swabs only from both tube and cavity models. Experiments were performed 10 and 3 times for VFA and SARS-CoV-2 RNA, respectively (ns is $p > 0.05$, * is $p \leq 0.0332$, ** is $p \leq 0.0021$).

Model	Virus	Swab type	Ct (±SD)	Ct HEX [N1] (±SD)	Ct FAM [N2] (±SD)
Cavity	YFV	Heicon	30.08 ± 1.17	–	–
		Commercial	31.48 ± 1.76	–	–
	SARS-CoV-2	Heicon	–	27.00 ± 2.86	27.68 ± 1.16
		Commercial	–	28.64 ± 1.41	28.41 ± 0.94
Tube	YFV	Heicon	25.91 ± 0.93	–	–
		Commercial	26.69 ± 1.46	–	–
	SARS-CoV-2	Heicon	–	23.59 ± 2.99	22.89 ± 2.20
		Commercial	–	24.52 ± 0.97	24.82 ± 0.92

Table 2. Ct values for YFV and SARS-CoV-2 taken with Heicon and commercial nasopharyngeal swabs from both tube and cavity models.

swab releases back into medium the highest possible percentage of the volume of cellular material collected. Failing to do so will result in unreliable molecular test data or even failing to pass the sensitivity thresholds.

Regarding cost-effectiveness, preliminary analysis suggests potential economic advantages of the Heicon design. The injection molding process enables high-volume production with cycle times of 10–30 s per part, while the single-material polypropylene construction eliminates secondary fiber application processes, potentially reducing manufacturing costs by 30–50% compared to flocked swabs. The use of readily available medical-grade materials and standard manufacturing equipment also enables local production, reducing supply chain dependencies that proved critical during pandemic conditions. However, comprehensive health economic evaluation including regulatory costs, clinical validation expenses, and long-term performance outcomes would be required for definitive cost-effectiveness determination.

The cavity and tube models were validated using two viral targets (YFV and SARS-CoV-2) to assess swab performance under different virological and molecular detection conditions. The consistent Ct differences observed for both viruses across anatomical and simplified models support the model's robustness and its utility in pre-clinical validation protocols for respiratory pathogens. The results reinforce that this model not only reflects anatomical complexity but also provides sensitivity to detect variations in swab performance across different diagnostic contexts. Several studies have found similar results of virus-loaded sample collection when performing comparative analysis between injection and flocked nasopharyngeal swabs. For example, Ghezzi et al. loaded a cellulose sponge with a 2% polyethylene oxide solution containing SARS-CoV-2 at a concentration of 10^6 copies/mL[2]. Their results showed that the injected swab had a shorter cycle time (34.00) than the flocked swab (39.00)[2]. Differences are also observed in the Ct values of mucosal substitute samples developed with silk sponge loaded with 0.5% polyethylene oxide and 10^5 copies/mL of SARS-CoV-2 taken with flocked (36.5) and injected (38) swabs in a nasopharyngeal cavity model without the external nasal anatomy[1]. The fact that significantly better results are presented with the flocked swab may be a result of the lack of an external nasal

region, as the vestibule surfaces have been shown to have significant effects on sample collection and release[21]. Additionally, the Heicon-type swab demonstrated higher release efficiency, which can be attributed to several material science principles. The injection-molded polypropylene surface exhibits lower surface energy compared to nylon fibers, reducing adhesive interactions with the hydrogel matrix[22]. The smooth surface topology (surface roughness $Ra \approx 0.5–2.0$ µm) provides adequate mechanical retention during collection while minimizing deep retention sites that resist sample release[23]. Furthermore, the dimensional stability of polypropylene in aqueous environments ensures consistent release performance throughout the sample transport process, unlike hygroscopic materials that may alter their geometry upon fluid exposure[22].

Additionally, the simulation of the nasopharyngeal mucosa with hydrogels allows a better integration of the components[24] and thus a better uptake of the viral material during swabbing. Importantly, the lack of amplification of the RNase P gene in the samples indicates the absence of cellular material. The results indicate that there is no statistically significant difference between the positive control of the kit and the nasopharyngeal cavity (FAM and HEX channels, $p > 0.0868$), which demonstrates that the RNA collected meets the requirements to be classified as an intact sample. These results demonstrate that the SISMA hydrogel not only supports RNA preservation and extraction but also enables discrimination between swab performance under realistic anatomical conditions, thereby validating its use as a physiologically relevant mucosal substitute. The kit's positive and negative controls showed the expected results, i.e., cycle times less than 27 on the FAM and HEX channels and no detection in the Cy5 channel for the positive and no detection on any channel for the negative. The positive control in cavity presents significantly lower Ct values (18.21 in FAM and 18.88 in HEX for Heicon; 19.41 in FAM and 19.32 in HEX for commercial) than those mentioned for the samples, which indicates that the developed test bank largely avoids false positives in the clinical test results even in close proximity to the acceptance limit. This study underscores the importance of employing anatomically and physiologically accurate models in the pre-clinical assessment of nasopharyngeal swabs, which is crucial for the development of diagnostic tools during pandemics.

However, the model has inherent limitations that must be acknowledged for proper interpretation of results. From a physiological perspective, it does not incorporate dynamic components such as mucociliary clearance, which could affect viral particle distribution and retention[25]. The model also lacks temperature regulation (maintained at room temperature rather than physiological 37 °C), humidity control, and the complex biochemical environment of active mucosa including immune components, cellular debris, and enzymatic activity that can influence viral stability and swab-mucus interactions[26–28]. From a materials science standpoint, the SISMA hydrogel, while rheologically matched to human mucus, represents a simplified polymer network that may not fully capture the complex glycoprotein structure and viscoelastic recovery characteristics of native mucin. Additionally, the dual-material 3D printing approach, though anatomically accurate, creates discrete material interfaces rather than the gradual tissue property transitions found in vivo. The hydrogel may also exhibit time-dependent behavior including potential dehydration, cross-linking changes, or microbial contamination that could affect reproducibility across extended testing periods. Despite these limitations, the model demonstrates robust performance as a standardized platform for comparative swab evaluation, offering superior physiological similarity compared to simple tube-based methods while maintaining the reproducibility essential for pre-clinical device validation.

In conclusion the 3D printed cavity model demonstrated superior efficacy in sample release compared to the standard tube model, suggesting its enhanced suitability for pre-clinical validation of nasopharyngeal swabs. Crucially, the research contributes significant advancements to the realm of pre-clinical testing for nasopharyngeal swabs. By integrating a realistic 3D printed anatomical structure with a SISMA hydrogel, we have observed noteworthy distinctions between the novel cavity model and the conventional tube model. The cavity model offers a more accurate representation of the nasal anatomy, which is paramount for the precise pre-clinical validation of swabs used in the diagnosis of viral infections. In summary, the application of a more anatomically and mechanically faithful model for evaluating nasopharyngeal swabs could substantially refine their design and functionality. This, in turn, would enhance the reliability and efficacy of diagnostic tests for detecting nasopharyngeal pathogens, including SARS-CoV-2. The findings underscore the importance of anatomical and physiological accuracy in pre-clinical testing, which may lead to improved clinical outcomes and public health responses during viral outbreaks.

Future work should focus on systematic validation progression toward clinical implementation. Immediate next steps include testing with more complex biological matrices such as spiked sputum samples and mucus with varying pathological viscosity profiles, followed by ex vivo validation using fresh human tissue samples to provide intermediate validation while maintaining experimental control. Although this model is designed for early-stage pre-clinical validation, the eventual transition to clinical studies would require carefully designed comparative trials following Good Clinical Practice guidelines, focusing initially on analytical performance parameters including sensitivity, specificity, and correlation with established reference methods across diverse patient populations. In this context, a comprehensive Limit of Detection (LoD) study comparing the Heicon swab with established clinical swabs represents a critical next validation phase. This would involve systematic serial dilution testing across 6–8 viral concentration levels using both SARS-CoV-2 and YFV systems, following CLSI EP17-A2 guidelines for analytical sensitivity determination. The study design would establish 95% detection probability thresholds for each swab type in both anatomically accurate and simplified models, using probit regression analysis to determine statistical confidence intervals. Beyond analytical LoD assessment, such studies would evaluate clinical diagnostic sensitivity by incorporating collection efficiency, release kinetics, and matrix effects to provide comprehensive performance benchmarking. These analytical validation studies are essential prerequisites for regulatory submission and would provide quantitative evidence supporting clinical utility claims and eventual translation into diagnostic practice.

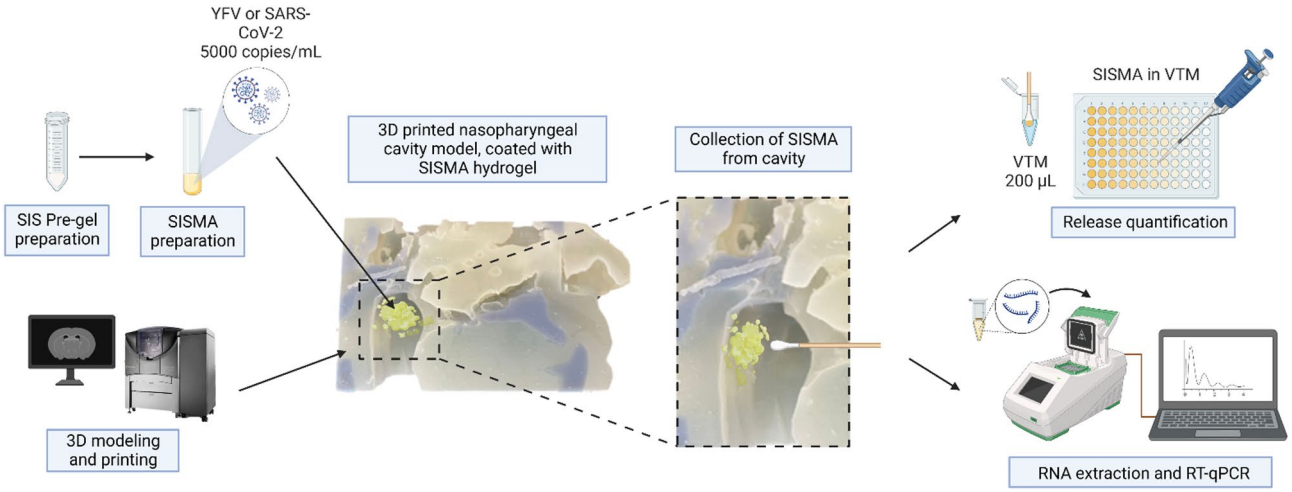

Fig. 5. Protocol summary for model preparation and nasopharyngeal swab testing in the nasopharyngeal cavity. The same protocol was used for the control sampling standard in Eppendorf tubes.

Materials and methods

Swab acquisition and Preparation

Heicon-type swabs (Heicon swabs) were manufactured via one-step injection by Plastinovo S.A.S. (La Estrella, Colombia) and sterilized using ethylene oxide (100%, 100 g, 18 h, 38–55 °C). Commercial nylon flocked I Swabs (Commercial swabs) were purchased from HanChang Medic Co. Ltd (Seoul, Korea) and from Changzhou Munk Foam Technology Co. Ltd (Jiangsu, China). The swabs were directly taken from the original sterilized packaging for immediate testing. Swab use and the overall protocol of the study are summarized in Fig. 5.

SISMA hydrogel preparation

Pre-gel preparation and biochemical modification

Porcine small intestinal submucosa (SIS) powder was prepared and modified following the protocol previously reported[12]. Briefly, SIS powder (obtained following the protocol described in[29] was solubilized at 4 mg/mL in a solution of 0.5 M glacial acetic acid (PanReac AppliChem, Chicago, IL, USA) and 1 mg/mL porcine pepsin (PanReac AppliChem, Chicago, IL, USA) under vigorous magnetic stirring at room temperature for 48 h. A functional solution of methacrylic acid (MA, Sigma-Aldrich, St. Louis, MO, USA), 1:20 molar excess with respect to free amines in SIS), 1-ethyl-3-(3-dimethylaminopropyl) carbodiimide hydrochloride (EDC, Sigma-Aldrich, St. Louis, MO, USA, 1:1 molar ratio with respect to MA) and N-hydroxysuccinimide (NHS, Sigma-Aldrich, St. Louis, MO, USA, 1:1 molar ratio with respect to MA) was prepared in N, N-dimethylformamide (DMF, Sigma-Aldrich, St. Louis, MO, USA) and heated for 15 min at 40 °C under constant magnetic stirring. The functional solution was mixed with the SIS pre-gel (1:1 volume ratio) for 24 h under constant magnetic stirring at 4 °C. The MA-modified SIS hydrogel (SISMA) was dialyzed against 0.25 M acetic acid for 48 h with 100 times the volume of SISMA and lyophilized for 96 h.

Hydrogel preparation

The formulation and the measurement of rheological properties of the SISMA hydrogel have been previously reported by our research group[12]. Briefly, a functional solution (pH 8.5) consisting of DMEM Low Glucose (BioWest S.A.S., Nuaillé, France) supplemented with 0.1% (w/v) riboflavin (RF, Sigma-Aldrich, St. Louis, MO, USA) and 0.1 M Tris-HCl, (PanReac AppliChem, Chicago, IL, USA) was prepared. Lyophilized SISMA was resuspended at 40 mg/mL in 0.02 M glacial acetic acid. The DMEM and SISMA solutions were mixed at a 1:1 volume ratio for 15 min under constant magnetic stirring at 4 °C. Rheological properties were measured using a Discovery Series Hybrid Rheometer-1 (TA Instruments, New Castle, DE, USA) with parallel plate geometry, 20 mm gap between plates, shear rates from 0.01 to 200 1/s at 1% strain and room temperature. The resulting plot of viscosity (η) versus shear rate (γ) was fit to the power law $\eta = K\gamma^{n-1}$, where η corresponds to the viscosity, γ to the shear rate, and K and n to shear thinning coefficients.

Binding of the SISMA hydrogel to the viral material

Yellow fever virus vaccine (YFV) YFV (Stamaril®, Sanofi Pasteur, Lyon, France) containing live attenuated virus strain 17D-204 propagated in chick embryos with 1000 infectious units (IU) LD50 was diluted to a concentration of 5000 copies/mL using Eqs. (1) and (2)[30]. A YFV to DMEM-SISMA (20:80 (v/v)) mixture was made and stored at -20 °C until further use. This concentration was selected to simulate a clinically relevant viral load commonly observed in early symptomatic stages of infection and lies above the lower detection threshold of standard RT-qPCR assays[31,32], ensuring reliable detection while avoiding signal saturation.

$$1\mathrm{IU} = 1.91\mathrm{PFU} \tag{1}$$

$$\text{Log10 PFU/mL} = (0.974 * \text{Log10} * \text{copies/mL}) - 2.807 \quad (2)$$

SARS-CoV-2 viral material (SARS-CoV-2) SARS-CoV-2 (AccuPlex™ SARS-CoV-2 Reference Material Kit, SeraCare Life Sciences Inc., Milford, MA, USA) at a concentration of 5000 copies/mL was mixed with DMEM-SISMA (20:80 (v/v)). The final solution was stored at -20 °C until further use. The selected viral load corresponds to the working dilution of the certified reference material and mirrors the concentration used for YFV to ensure consistency across assays and traceability to international reference standards.

3D printed nasopharyngeal cavity

A three-dimensional digital reconstruction of the nasopharyngeal cavity was built from computed tomography (CT) images of anonymous adult patients from the open-access NIH Database (USA), using Mimics® and 3-Matic® software packages (Materialise, Belgium). Soft tissue structures and bones were segmented considering Hounsfield radiodensity units of + 700 for cancellous bone and + 3000 for dense bone[33]. The anatomical model was co-printed on the Stratasys Objet260 Connex 1 3D printer (Stratasys, MN) at the Center for Modeling and 3D Printing (Fundación Cardioinfantil – Instituto de Cardiología, Bogotá, Colombia). Flexible, translucent material (Agilus30™) was used for the soft tissues, and rigid, blue material (VeroBlue™) was used for the bones.

Standardization of collection test in the 3D printed cavity

A standardized protocol was developed to compare the performance of two nasopharyngeal swabs in sample collection from the 3D printed cavity. For this, 200 µL of SISMA hydrogel was deposited on the nasopharyngeal area within cavity. Following the Center for Disease Control and Prevention (CDC) recommendations for upper respiratory tract sampling[34], each swab was weighed before insertion through the nostril, parallel to the palate, until resistance indicated correct positioning. Once in contact with the hydrogel, the swabs were rotated 5 times clockwise and counter-clockwise, maintaining contact with the cavity wall for 10 s to ensure thorough absorption of the secretion analogue. Post-rotation, swabs were carefully removed with a rotation motion and reweighed. The sample collection efficacy of the swabs was calculated by the mass difference between pre- and post-swabbing. The volume of sample collected was extrapolated from its mass and the known density of the SISMA hydrogel, using 1 mL as the standard volume measure. The collected sample volumes were statistically analyzed with Graph Pad Prism 9® software, applying Student's t-test ($n = 5$).

Standardization of collection test in tube

For comparison, a standard collection test was conducted in a tube environment for benchmarking. For this, an aliquot of 200 µL of SISMA hydrogel was placed in an Eppendorf tube, and the swab was inserted, touching the tube's bottom, followed by the same rotation and holding protocol described above (see Standardization of collection test in the 3D printed cavity). Finally, the swab's collection capacity was determined following the same weight differential protocol described above (see Standardization of collection test in the 3D printed cavity).

Release test standardization

Both the Heicon and commercial swabs, post-collection, were broken at the predesign breakpoint. The swab heads were immersed in 300 µL of viral transport medium (VTM) to facilitate the release of the SISMA hydrogel loaded with either YFV or SARS-CoV-2. The VTM mixtures, i.e., VTM-SISMA-YFV or VTM-SISMA-SARS-CoV-2 were subsequently transferred into a FLUOstar® Omega microplate for absorbance (Abs) reading (BMG Labtech Inc, Ortenberg, Germany) at 405 nm. Controls were established, with the positive control (PC) containing the average collected SISMA volume in VTM and the negative control (NC) containing VTM alone. The average collected SISMA volumes were determined from the mass differences in the swab collection assays (see Sect. 4.4 and 4.5) and were subsequently pipetted into the VTM for the preparation of the respective PC. The released percentage was calculated using the following equation: ((Sample Abs-NC Abs)/(PC Abs-NC Abs)) x100. These measurements were analyzed with Graph Pad Prism 9® software and Student's T-test ($n = 5$).

Viral RNA extraction

The extraction process for viral RNA from samples began with a treatment of 200 µL of VTM-SISMA-YFV or VTM-SISMA- SARS-CoV-2 with 25 µL of proteinase K at room temperature to degrade viral capsid proteins and deactivate potential RNA-degrading nucleases. Subsequently, 200 µL of lysis buffer was added and vortexed for 15 s. The mixture was then incubated at 56 °C for 15 min. The subsequent RNA purification followed the Monarch® Total RNA Miniprep kit protocol. Briefly, 400 µL of the sample was transferred to a gDNA removal column in a 1.5 mL Eppendorf tube. A first centrifugation was performed at 16000xg for 30 s and 400 µL of 97% ethanol was pipetted onto the supernatant. The sample and ethanol mixture were transferred to an RNA purification column in a 1.5 mL Eppendorf tube and centrifuged again at 16000xg for 30 s, discarding the supernatant. Then, 500 µL of RNA wash buffer was added and centrifuged at 16000xg for 30 s, discarding the supernatant. Immediately, 5 µL of DNase I was added with 75 µL of DNase I reaction buffer and incubated for 15 min at room temperature. 500 µL of priming buffer was added to the sample and centrifuged at 16000xg for 30 s. A second RNA wash was performed with a volume of 500 µL, centrifuged at 16000xg for 2 min and the column was transferred to an RNase-free tube. Purified RNA was eluted from the column with 30 µL of nuclease-free water followed by centrifugation at 16000xg for 30 s. The supernatant contained purified RNA, which was maintained on an ice bath at -20 °C for later use. The concentration of the resultant RNA was quantified at an optical density of 260/280 with the DS-11 spectrophotometer (DeNovix, Wilmington, DE, USA). The data obtained were statistically analyzed with Graph Pad Prism 9® software and Student's T-test ($n = 10$).

RT-qPCR testing

RT-qPCR assays were conducted for both YFV and SARS-CoV-2 RNA. For YFV, the assay was performed in a total reaction volume of 15 µL that comprised 0.6 µL of forward primer GGGACTAGCGT- GATCATTGA, 0.6 µL of reverse primer GAATAACTTTTTCC- CGCTATCCGT[35] (0.4 µM, Macrogen, Seoul, Republic of Korea), 0.75 µL of enzyme mix, 7.5 µL of reaction mix, and 5.25 µL of YFV RNA as specified by Luna® Universal One-Step RT-qPCR Kit protocol. SARS-CoV-2 was assayed using the Luna® SARS-CoV-2 RT-qPCR Multiplex Assay Kit. The samples tested included experimental groups and positive and negative controls for the kit. For these, 3.75 µL of enzyme mix and 1.5 µL of primer/probe mix were used. For experimental samples, 2.25 µL of nuclease-free water and 7.5 µL of SARS-CoV-2 RNA were added. For the positive control, 8.25 µL of nuclease-free water and 1.5 µL of a plasmid DNA containing the SARS-CoV-2 N gene were added. For the negative control, 9.75 µL of nuclease-free water was added. The mixtures were centrifuged for 1 min at 2500 rpm to eliminate bubbles. RT-qPCR cycling began with a reverse transcription at 55 °C for 10 min, followed by an initial denaturation at 95 °C for 1 min. This was succeeded by 40 denaturation cycles at 95 °C for 10 s and 50 extension cycles at 60 °C for approximately 30 s. Fluorophore responses for YFV RNA were monitored on the green channel, while for SARS-CoV-2, responses for the N2 region, human RNase P gene, and the N1 region were monitored on the green, red, and yellow channels, respectively. Ct values obtained for each sample were evaluated with Graph Pad Prism 9® software and Student's t-test ($n = 10$ for YFV and $n = 3$ for SARS-CoV-2).

Data availability

The datasets generated during and/or analyzed during the current study are available from the corresponding author on reasonable request.

Received: 8 May 2025; Accepted: 18 September 2025
Published online: 23 October 2025

References

1. Hartigan, D. R. et al. In vitro nasal tissue model for the validation of nasopharyngeal and midturbinate swabs for SARS-CoV-2 testing. *ACS Omega*. **7**, 12193–12201. https://doi.org/10.1021/acsomega.2c00587 (2022).
2. Ghezzi, C. E. et al. Preclinical validation of a novel Injection-Molded swab for the molecular assay detection of SARS-CoV-2. *Diagnostics* **12**, 206. https://doi.org/10.3390/diagnostics12010206 (2022).
3. Lai, S. K., Wang, Y-Y., Wirtz, D. & Hanes, J. Micro- and macrorheology of mucus. *Adv. Drug Deliv Rev.* **61**, 86–100. https://doi.org/10.1016/j.addr.2008.09.012 (2009).
4. Miyabe, Y. et al. Aggregated eosinophils characterize airway mucus properties. MedRxiv 2022:2022.11.15.22282331. https://doi.org/10.1101/2022.11.15.22282331
5. Dutta, N. & Dhar, D. Understanding medical technology innovation in Low- and Middle-Income countries: Factors, Impact, and a model proposal. *She Ji: J. Des. Econ. Innov.* **10**, 192–222. https://doi.org/10.1016/j.sheji.2024.07.002 (2024).
6. 3D Solutions S.A.S. Kit para la toma de muestras diagnósticas del COVID-19. (Impresión 3D Colombia). 3D Solutions SAS (2021). https://www.3dsolutions.com.co/single-post/2020/08/05/kit-para-la-toma-de-muestras-diagn%C3%B3sticas-del-covid-19-impresi%C3%B3n-3d-colombia?srsltid=AfmBOooVjLf4KoptvVgH8v9JS-YB4Qn3tfte6TL6w_lVlxdrrDocbgYz
7. Moreno Castañeda, L. C. Tecnovigilancia en el Contexto de la Pandemia COVID-19 – Dispositivos Médicos Vitales No Disponibles. Bogotá: (2021).
8. Stratasys Ltd & Vero for Stratasys, J. :1–1. (2020). https://www.stratasys.com/siteassets/materials/materials-catalog/polyjet-materials/verovivid/mds_pj_vero_for_j55_0320a.pdf
9. Zerdzicki, K. et al. Tensile modulus of human orbital wall bones cut in sagittal and coronal planes. *PLoS One*. **16**, e0259363. https://doi.org/10.1371/journal.pone.0259363 (2021).
10. Stratasys Ltd Agilus30. :1–1. (2021). https://www.stratasys.com/globalassets/materials/materials-catalog/polyjet-materials/agilus30/mds_pj_agilus30_0121b.pdf
11. Spahn, G. et al. Mechanical behavior of intact and low-grade degenerated cartilage. *Biomedizinische Technik/Biomedical Eng.* **52**, 216–222. https://doi.org/10.1515/BMT.2007.039 (2007).
12. Rueda-Gensini, L., Serna, J. A., Cifuentes, J., Cruz, J. C. & Muñoz-Camargo, C. Graphene Oxide-Embedded extracellular Matrix-derived hydrogel as a multiresponsive platform for 3D Bioprinting applications. *Int. J. Bioprint*. **7**, 124–139. https://doi.org/10.18063/ijb.v7i3.353 (2021).
13. Kalinowski, M. J., Hartigan, D. R., Lojek, N. M., Buchholz, B. O. & Ghezzi, C. E. Underscoring the effect of swab type, workflow, and positive sample order on swab pooling for COVID-19 surveillance testing. *Sci. Rep.* **13**, 7174. https://doi.org/10.1038/s41598-023-34337-y (2023).
14. Tay, J. K. et al. Design and multicenter clinical validation of a 3-Dimensionally printed nasopharyngeal swab for SARS-CoV-2 testing. *JAMA Otolaryngology–Head Neck Surg.* **147**, 418. https://doi.org/10.1001/jamaoto.2020.5680 (2021).
15. McCarthy, A. et al. Ultra-absorptive nanofiber swabs for improved collection and test sensitivity of SARS-CoV-2 and other biological specimens. *Nano Lett.* **21**, 1508–1516. https://doi.org/10.1021/acs.nanolett.0c04956 (2021).
16. Sobiesk, J. L., Munakomi, S. & Anatomy *Head and Neck, Nasal Cavity* (StatPearls Publishing, 2023).
17. Mamba'udin, A., Handayani, M., Triawan, F., Rahmayanti, Y. D. & Muflikhun, M. A. Excellent characteristics of environmentally friendly 3D-Printed nasopharyngeal swabs for medical sample collection. *Polym. (Basel)*. **15**, 3363. https://doi.org/10.3390/polym15163363 (2023).
18. van der Elst, L. A., Gokce Kurtoglu, M., Leffel, T., Zheng, M. & Gumennik, A. Rapid fabrication of sterile medical nasopharyngeal swabs by stereolithography for widespread testing in a pandemic. *Adv. Eng. Mater.* **22**, 1–12. https://doi.org/10.1002/adem.202000759 (2020).
19. Todsen, T. et al. Valid and reliable assessment of upper respiratory tract specimen collection skills during the COVID-19 pandemic. *Diagnostics* **11**, 1987. https://doi.org/10.3390/diagnostics11111987 (2021).
20. Sananès, N. et al. 3D-printed simulator for nasopharyngeal swab collection for COVID-19. *Eur. Arch. Otorhinolaryngol.* **278**, 2649–2651. https://doi.org/10.1007/s00405-020-06454-1 (2021).
21. Warnke, P., Frickmann, H., Ottl, P. & Podbielski, A. Nasal screening for MRSA: different Swabs – different Results! *PLoS One*. **9**, e111627. https://doi.org/10.1371/journal.pone.0111627 (2014).
22. Elsebaei, A., Fayed, H., Elshaer, M. & Mobasher, M. Improvements in surface properties of Polypropylene, polycarbonate and polyurethane by nonthermal atmospheric pressure plasma Arc jet in air. *Egypt. Int. J. Eng. Sci. Technol.* **44**, 68–79. https://doi.org/10.21608/eijest.2023.176321.1198 (2023).

23. Ovhal, M. & Bahadur Balwanshi, J. Experimental investigation of surface roughness of polypropylene polymer using TNMG insert. *J. Harbin Eng. Univ.* **44**, 1653–1666 (2023).
24. Thang, N. H., Chien, T. B. & Cuong, D. X. Polymer-Based hydrogels applied in drug delivery: an overview. *Gels* **9**, 523. https://doi.org/10.3390/gels9070523 (2023).
25. Bailey, L. Aging diminishes mucociliary clearance of the lung. *Adv. Geriatr. Med. Res.* **4**, 1–12. https://doi.org/10.20900/agmr20220005 (2022).
26. Bisht, K. & te Velthuis, A. J. W. Decoding the role of temperature in RNA virus infections. *MBio* **13** https://doi.org/10.1128/mbio.02021-22 (2022).
27. Mettelman, R. C., Allen, E. K. & Thomas, P. G. Mucosal immune responses to infection and vaccination in the respiratory tract. *Immunity* **55**, 749–780. https://doi.org/10.1016/j.immuni.2022.04.013 (2022).
28. Li, X. et al. The intricate interplay among microbiota, mucosal immunity, and viral infection in the respiratory tract. *J. Transl Med.* **23**, 488. https://doi.org/10.1186/s12967-025-06433-2 (2025).
29. Sánchez-Palencia, D. M., D'Amore, A., González-Mancera, A., Wagner, W. R. & Briceño, J. C. Effects of fabrication on the mechanics, microstructure and micromechanical environment of small intestinal submucosa scaffolds for vascular tissue engineering. *J. Biomech.* **47**, 2766–2773. https://doi.org/10.1016/j.jbiomech.2014.04.048 (2014).
30. Bonin, C. R. B. et al. Validation of a yellow fever vaccine model using data from primary vaccination in children and adults, re-vaccination and dose-response in adults and studies with immunocompromised individuals. *BMC Bioinform.* **21**, 551. https://doi.org/10.1186/s12859-020-03845-3 (2020).
31. Buchta, C. et al. Results of a SARS-CoV-2 virus genome detection external quality assessment round focusing on sensitivity of assays and pooling of samples. *Clin. Chem. Lab. Med. (CCLM).* **60**, 1308–1312. https://doi.org/10.1515/cclm-2022-0263 (2022).
32. Moradi Marjaneh, M. et al. Analysis of blood and nasal epithelial transcriptomes to identify mechanisms associated with control of SARS-CoV-2 viral load in the upper respiratory tract. *J. Infect.* **87**, 538–550. https://doi.org/10.1016/j.jinf.2023.10.009 (2023).
33. Bibb, R., Eggbeer, D. & Paterson, A. *Medical imaging. Medical Modelling: the Application of Advanced Design and Rapid Prototyping Techniques in Medicine* 2nd edn p. 7–34 (Woodhead Publishing, 2015). https://doi.org/10.1016/B978-1-78242-300-3.00002-0
34. Centers for Disease Control and Prevention. Centers for Disease Control and Prevention. Interim Guidelines for Collecting and Handling of Clinical Specimens for COVID-19 Testing 2022. accessed February 10, (2023). https://www.cdc.gov/coronavirus/2019-ncov/lab/guidelines-clinical-specimens.html
35. Fischer, C. et al. Lineage-Specific Real-Time RT-PCR for yellow fever virus outbreak Surveillance, Brazil. *Emerg. Infect. Dis.* **23**, 1867–1871. https://doi.org/10.3201/eid2311.171131 (2017).

Acknowledgements

The authors extend their gratitude to the Biomedical Engineering Department at Universidad de los Andes (Bogotá, Colombia) and to the Center for Modeling and 3D Printing at Fundación Cardioinfantil – Instituto de Cardiología (Bogotá, Colombia) for 3D printing of the nasopharyngeal cavity anatomical model and early prototypes, and to Rodrigo Cabrera at Pontificia Universidad Javeriana (Bogotá, Colombia) for providing the viral transport media. Equally, we express our gratitude to Plastinovo S.A.S for the provision of the Heicon swabs.

Author contributions

I.C.O.-G. conceptualised the study, curated and analysed the data, conducted the investigation, developed the methodology, performed the software analysis, created visualisations, and wrote the original draft. I.M.F.-C. curated and analysed the data, conducted the investigation, developed the methodology, created visualisations, and contributed to writing the original draft. M.A.A. contributed to the investigation and methodology. M.A.R.-S. curated and analysed the data, conducted the investigation, and developed the methodology. C.E.P.-C. contributed to the software development, methodology, and visualisations. C.I.C.-P. supervised the study, validated the findings, and reviewed and edited the manuscript. J.C.C. conceptualised the study, developed the methodology, managed the project, provided resources, supervised the study, validated the findings, and reviewed and edited the manuscript. C.M.-C. supervised the study, validated the findings, and reviewed and edited the manuscript. J.N. contributed to the methodology, managed the project, provided resources, supervised the study, validated the findings, and reviewed and edited the manuscript. R.C. provided resources, supervised the study, validated the findings, and reviewed and edited the manuscript. J.C.B. acquired funding, managed the project, provided resources, supervised the study, validated the findings, and reviewed and edited the manuscript. All authors reviewed and approved the final manuscript.

Funding

This study "Prototipado rápido, pruebas, y escalado de soluciones basadas en manufactura aditiva para insumos COVID-19 y post-COVID-19" received funding from Universidad de los Andes, Universidad del Rosario and Pontificia Universidad Javeriana. The project involving the Center for Modeling and 3D Printing at Fundación Cardioinfantil – Instituto de Cardiología (Bogotá, Colombia) and the development of the anatomical models is funded by the Colombian Ministry of Science - MinCiencias (Ministerio de Ciencia, Tecnología e Investigación) under contract 744–2021 (Project code #223989785090).

Declarations

Competing interests

The authors declare no competing interests.

Additional information

Correspondence and requests for materials should be addressed to I.C.O.-G.

Reprints and permissions information is available at www.nature.com/reprints.

Publisher's note Springer Nature remains neutral with regard to jurisdictional claims in published maps and institutional affiliations.